

# Imaging of Surface Plasmon and Ultrafast Dynamics in Gold Nanorods by Near-Field Microscopy

Kohei Imura,<sup>†,‡</sup> Tetsuhiko Nagahara,<sup>†</sup> and Hiromi Okamoto<sup>\*,†,‡</sup>

*Institute for Molecular Science and The Graduate University for Advanced Studies, Okazaki 444-8585, Japan*

*Received: May 13, 2004; In Final Form: June 1, 2004*

We investigated the near-field optical properties of single gold nanorods. Transmission images observed near the surface plasmon resonances agree qualitatively with the calculated maps of the optical local density of states and are reflected by spatial characteristics of plasmon wave functions. Ultrafast temporal responses have been observed by combining near-field microscopy with a time-resolved technique. It has been found that the behavior of the collective motion of electrons in the center of the rod is different from that in both ends.

## Introduction

Scanning near-field optical microscopy (SNOM) has been extended over many fields of science.<sup>1,2</sup> The advantage of this method over conventional optical microscopy is its high spatial resolving power. Simultaneous topographic imaging is also advantageous. Recently, the feasibility of the imaging of the electromagnetic local density of states (LDOS) by SNOM has been demonstrated in a quantum dot and in optical corrals,<sup>3–5</sup> whereas the spatial distribution of the LDOS structure for a single particle has not been reported. LDOS is closely related to (or, under some circumstances, can be approximated to) the square moduli of wave functions of elementary excitations. Hence, the imaging of LDOS in a single particle by SNOM may lead to the direct optical observation of geometrical structures of wave functions. By combining with time-resolved techniques, ultrafast SNOM imagings give the dynamic behavior of LDOS after photoexcitation in a space- and time-resolved manner. It would be possible by the same principle to realize the manipulation of wave function to a specific target state.

In this letter, we focus on the static and time-resolved near-field optical imaging of LDOS in single gold nanorods (NRs). We show that LDOS structures in NRs observed by SNOM reflect the square moduli of surface plasmon (SP) eigenfunctions. We also investigate energy dissipation processes in an individual NR by dynamic imaging of the LDOS structure based on SNOM.

## Experimental Section

Gold NRs (diameter 15–40 nm) were synthesized chemically in solutions<sup>6</sup> and spin coated on a coverslip. A near-field microscope was operated under ambient conditions. The apertured near-field optical fiber probe (commercial) was etched and either aluminum or gold coated. The diameter of the probe aperture (50–100 nm) was determined either by a scanning electron microscope image or by the onset of the fluorescence signal from a dyed bead. The near-field probe was maintained in the vicinity of the sample surface by shear-force feedback, whose signal was used to construct a topographic image.

Morphologies of NRs were verified by topography measurements and/or by a scanning electron microscope.

A Xe discharge lamp and a Ti:sapphire laser ( $\lambda = 780$  nm,  $<100$  fs, 80 MHz) were used for transmission-spectral and time-resolved measurements, respectively.<sup>7</sup> For the transmission-spectral measurements, photons emerging from the near-field probe were collected by an objective and detected by a polychromator–CCD system. For time-resolved pump–probe measurements, the output from the laser was split into two beams, and both beams were mechanically chopped at different frequencies. The two optical beams were collinearly coupled to the other end of the near-field probe with an average power of 0.5–1.0 mW after precompensated group velocity dispersion arising from the optical fiber. The signal of interest was recovered through phase-sensitive detection at the difference of the chopping frequencies. The polarization of the pump and probe pulses was controlled by a quarter- and a half-wave plate.

## Results and Discussion

A shear-force topographic image of a NR is shown in Figure 1a. Figure 1b shows the transmission spectrum at the crossed point ( $\times$ ) under illumination conditions, where transmission is defined as  $-\Delta T = [I(\text{sub}) - I(\times)]/I(\text{sub})$ , where  $I(\times)$  and  $I(\text{sub})$  denote the measured intensities at the point  $\times$  and at the bare substrate, respectively. Dark counts of the detector were corrected. In the observed spectrum, two strong absorption bands are clearly seen. The broad, asymmetric shape of the peak around 850 nm in Figure 1b compared to that observed in the homogeneous environment<sup>8</sup> may be explained by the inhomogeneous environment around the NR on the substrate. Major features of the observation are in qualitative agreement with the low-spatial-resolution study.<sup>8</sup> Absorption bands near 520 and 850 nm can be assigned to transverse and longitudinal SP resonances, respectively. Polarization dependences for these bands confirmed the above assignment as shown in Figure 1c. Curves in the Figures indicate polarization angle dependences for a perfect dipole model. Transmission enhancement attributable to an antenna effect<sup>9</sup> is also found at 620 nm in the spectrum. The small absorption peak around 700 nm is ascribed to higher-order SP modes.<sup>10</sup>

Parts a and b of Figure 2 show the experimentally obtained optical near-field images at wavelengths of near-transverse (510

\* To whom correspondence should be addressed. E-mail: aho@ims.ac.jp.

<sup>†</sup> Institute for Molecular Science.

<sup>‡</sup> The Graduate University for Advanced Studies.

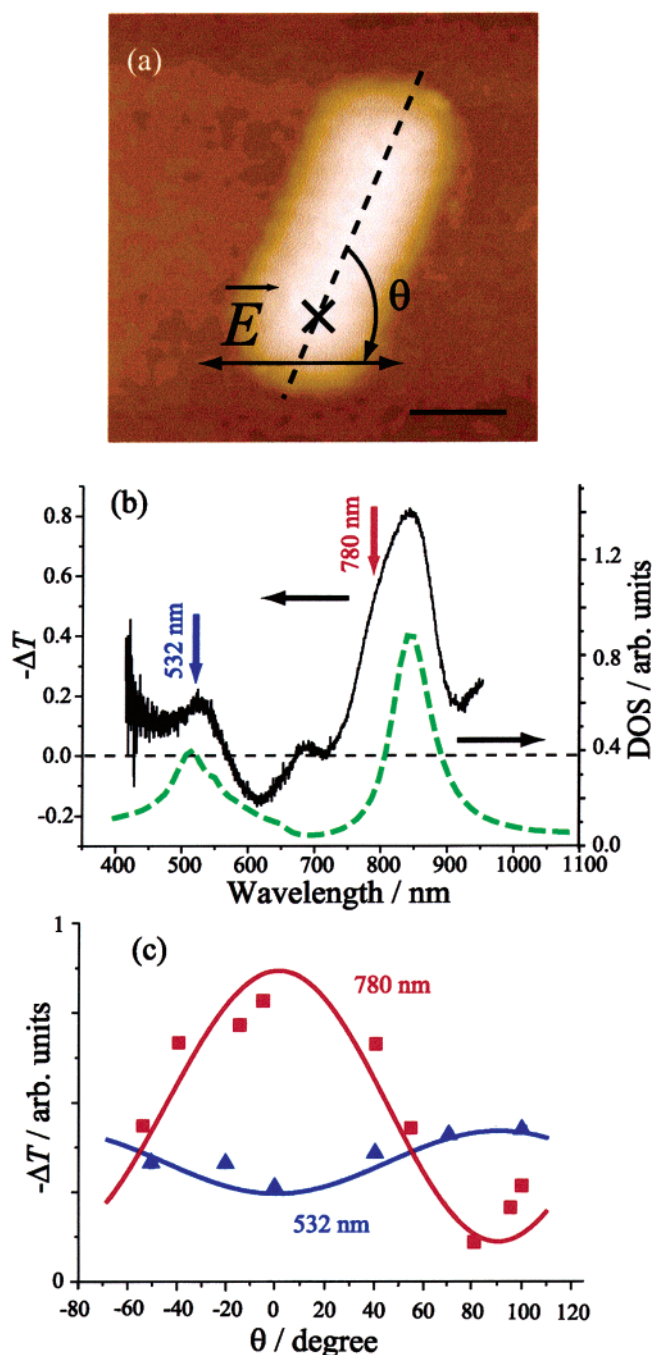


**Figure 1.** (a) Topography of a gold NR. Scale bar: 100 nm. (b) Transmission spectrum measured at point  $\times$  in part a (solid curve) and calculated DOS (dashed curve). (c) Polarization dependences of absorption for 532 and 780 nm at the point specified in part a.

nm) and longitudinal (780 nm) SP resonances. We estimated the spatial resolution in these images to be around 50–100 nm. To analyze the observed optical images of NR, we calculated the electromagnetic LDOS around the NR following the Green dyadic method in the literature.<sup>11–13</sup> LDOS can be extracted from the Green dyadic using the relation

$$\rho(\vec{r}, \omega) = -\frac{1}{\pi} \text{Tr}[\text{Im}\{\vec{G}(\vec{r}, \vec{r}, \omega)\}] \quad (1)$$

where  $\text{Tr}$  and  $\text{Im}$  stand for the trace and imaginary parts of Green dyadic  $\vec{G}(\vec{r}, \vec{r}, \omega)$ , respectively, and  $\vec{r}$  denotes the position of the NR.  $\vec{G}(\vec{r}, \vec{r}, \omega)$  can be solved numerically by the self-consistent discretized Dyson equation starting from the analyti-

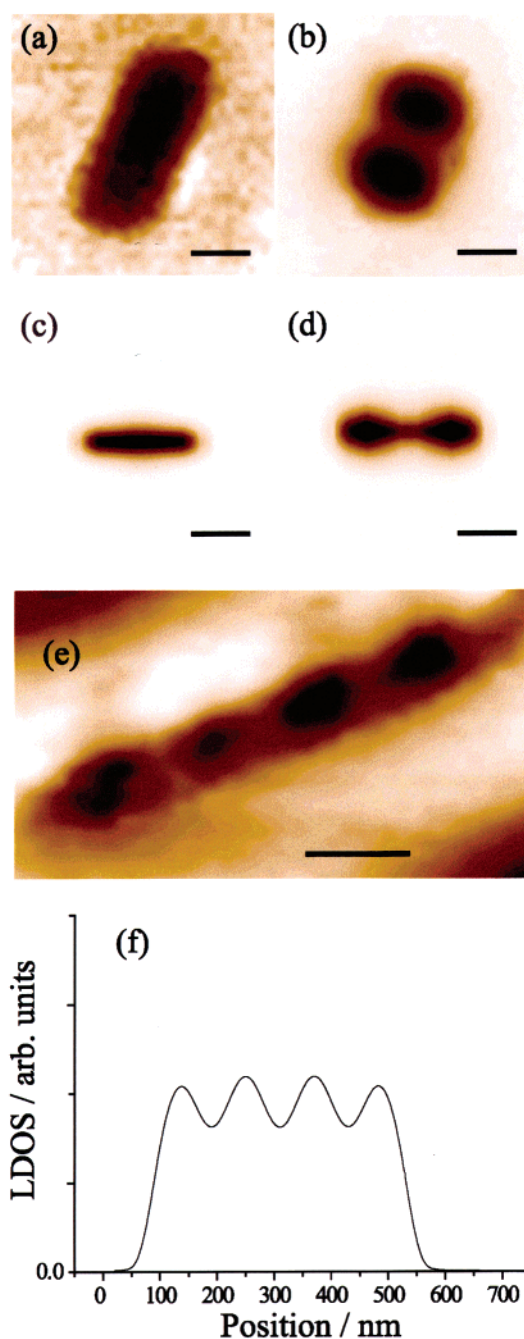


**Figure 2.** (a, b) Observed transmission images of a NR measured around 530 and 780 nm, respectively. (c, d) Calculated LDOS images of a NR corresponding to parts a and b, respectively. (e) Transmission image observed around 780 nm for a NR (length: 440 nm; diameter: 20 nm). (f) Calculated LDOS profile along the long axis of the NR. Scale bars: 100 nm.

cally known Green dyadic of the homogeneous medium.<sup>14</sup> In the present calculation, a cylindrical mesh was adopted, and the depolarizing effect in the source region (renormalization procedure) was also taken into account.<sup>15</sup>

Figure 1b shows the calculated spectrum of the DOS averaged over a NR. In accordance with the observation in Figure 1b, two distinct bands can be seen. Parts c and d of Figure 2 are the calculated LDOS images, corresponding to the observed ones in parts a and b of Figure 2 at 15 nm above the particle. The height (30 nm) and length (180 nm) of the NR used for the calculation was obtained from the topographic image by taking the convolution of the tip shape into account. Agreements between the observation and the calculation indicate the



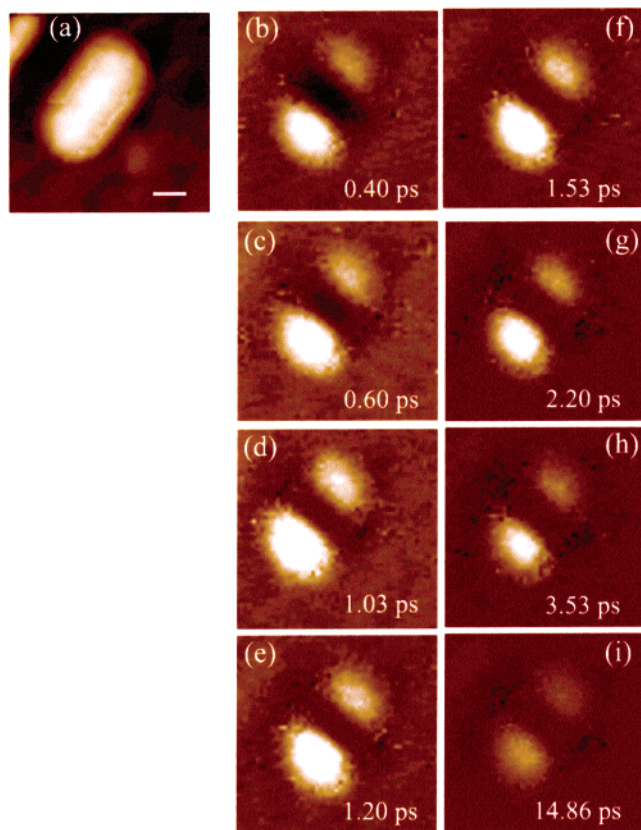


**Figure 3.** (a) Topography and (b–i) transient transmission images ( $\lambda = 780$  nm) of a NR taken at various pump–probe delay times. The delay time is indicated in each image. Scale bar: 100 nm.

successful imaging of LDOS structures in single NRs by SNOM and also suggest that effects of the near-field tip may be small compared to the interaction between radiation and the NR. The oscillating behavior of LDOS in a nanowire has been only predicted by numerical calculations.<sup>16,17</sup> We have experimentally found that the longer the rod length is, the more oscillation that appears. An example is given in Figure 2e. The calculated line profile of LDOS along the NR is shown in Figure 2f. For a larger NR of approximately 900 nm in length and 30 nm in diameter, up to 6 or 7 oscillation periods have been observed.

By definition, LDOS is closely related to the square moduli of the wave functions of elementary excitations (SP in the present case). The images presently observed should be interpreted as a visualization of LDOS, but they must be reflected by the characteristics of specific resonant SP modes. We have actually obtained an image with two humps in Figure 2b, which is interpreted as a result reflecting the character of the resonant SP wave function having a node at the center of the NR. Similarly, the image in Figure 2e must be relevant to the SP wave function with three nodes. In this sense, it may be said that the present results have enabled the optical observation of geometrical structures of wave functions of elementary excitations.

We proceed to the observation of the temporal LDOS behavior of NR by an ultrafast method combined with SNOM. It is of fundamental importance to know how the electron–electron (e–e) and electron–phonon (e–ph) scattering processes depend on the size and shape of nanoparticles and how they proceed inside the particle, and many attempts have been made to date.<sup>18–20</sup> One way to obtain a clear answer to these questions would be to use single-particle dynamic spectroscopy with high temporal and spatial resolution. Toward this goal, we combined

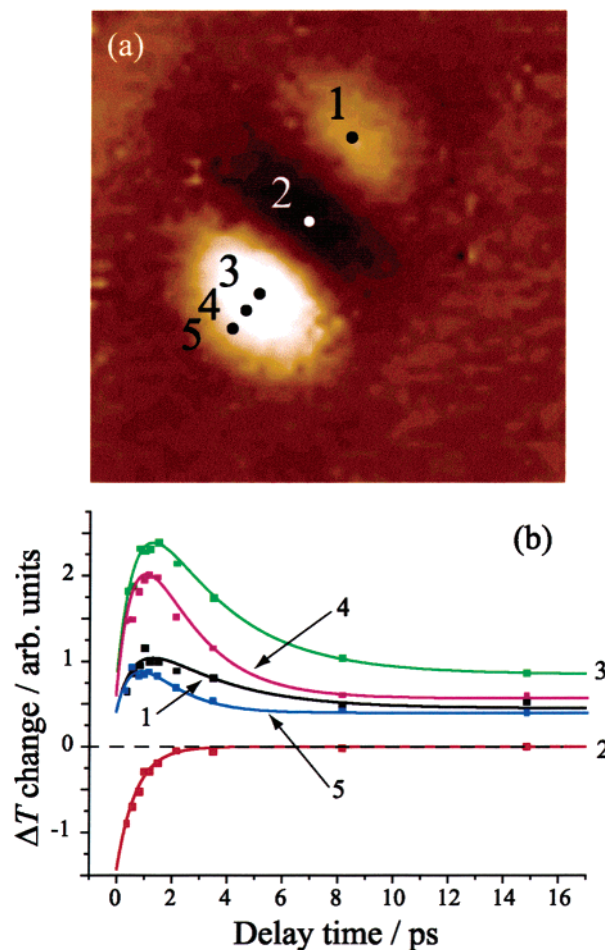


**Figure 4.** (a) Positions 1–5 to be analyzed. (b) Transient transmission changes as functions of delay time, converted from the data in Figure 3b–i. Solid curves indicate double- (for positions 1, 3, 4, and 5) and single- (for position 2) exponential fits, respectively.

SNOM with a pump–probe pulse correlation scheme to probing the ultrafast temporal behavior in a single NR. Near-infrared photons from the laser are used to perturb the energy distribution of the conduction electrons (via intraband absorption) and also to probe the energy dissipation processes. In this scheme, electron and phonon relaxation processes can be pursued by changing the pump–probe delay time, as imaged in Figure 3. The pump and probe fields are polarized along the long axis of the NR. The time resolution (ca. 100 fs) is limited by the pulse duration of the light source.<sup>7</sup> Bright and dark parts correspond to bleached absorption and induced absorption, respectively.

As clearly seen in Figure 3, the temporal response of the central part of the particle is different from those of both ends. Figure 4b shows time responses at positions 1 to 5 indicated in Figure 4a, as obtained from the spatiotemporal behavior shown in Figure 3. A fast rise and a slow decay are seen for positions 1, 3, 4, and 5. These temporal responses can be fit by double-exponential functions with steplike baselines that do not recover within the measured time range. The time constant for the faster component was found to be  $0.6 \pm 0.1$  ps, and that for the slower one was 2.8–1.5 ps (2.8 ps for positions 1 and 3, 1.8 ps for 4, and 1.5 ps for 5 with a typical uncertainty of  $\pm 0.3$  ps). The latter value is close to the values for e–ph relaxation obtained by ensemble measurements.<sup>20</sup> It may be reasonable to assign this picosecond signal decay to the e–ph process. Observed energy dissipation processes signify that the e–ph process (2.8–1.5 ps) shows internal position dependences in the NR. Although

the measured relaxation time contains experimental uncertainty, there is the definite reproducible tendency that the e-ph process becomes faster toward the end edge of the NR. This observation may be related to the different excitation efficiency near the edge of the NR because it is known that higher electronic temperatures give longer e-ph coupling times.<sup>21–23</sup> It is noted that the estimated fluence of the pump power (30–300  $\mu\text{J}/\text{cm}^2$ ) is comparable to that reported in the study of a 20-nm-thick gold film by Sun et al.<sup>24</sup> and corresponds to the maximum electronic-temperature change of  $\sim 300$  K. This partially explains the position-dependent e-ph relaxation. However, it is not clear whether the position-dependent excitation efficiency is sufficient to explain the whole range of effects. Other effects, such as electron-surface scattering, possibly have some influence, but they have not yet been identified because it has been reported that the e-ph process does not depend on particle size for gold spheres.<sup>21–23</sup> The fast (0.6-ps) process, which is observed uniformly in the NR including the center, may be attributed to the e-e process because a similar time response (0.5 ps) has been reported for the 20-nm-thick gold film.<sup>24</sup>

However, the slower decay component is hardly recognized at position 2, in contrast to the faster component. The lack of slower relaxation at the center is noteworthy but not straightforward to understand. When the light source is located at the center, only those SP modes with no node at the NR center, such as the in-phase mode, can be excited. In contrast, the SP mode with a node at the center is primarily excited at both ends of the NR, as mentioned before. If the excited state retains the memory of the initially excited SP mode, then the relaxation rate and/or optical character (absorbance change) for the e-ph relaxation might depend on the characteristics of the excited SP mode. (Otherwise, e-ph relaxation should be similar to that of the other positions.) Thus, the lack of e-ph relaxation at the center can be explained if the e-ph process after the excitation of the in-phase SP mode is very fast for some reason or if the absorbance change with relaxation is very small. If this is not the case, then the present observation should be attributed to the position dependence of the e-ph dynamics for other reasons, as discussed in the previous paragraph. Further investigation is needed to clarify the origin of the spatial-dependent dynamics.

## Conclusions

We report the static and time-resolved near-field optical imaging of LDOS in single gold nanorods with spatial resolution around 50–100 nm. Static optical images show characteristic spatial features of the surface plasmon mode and are in good agreement with the calculated local density of states. Spatiotemporal responses in the nanorod by the ultrafast SNOM technique reveal that the energy dissipation processes show characteristic position dependence. The electron-phonon relaxation becomes

faster toward the end edge of the NR. The present observation demonstrates that energy dissipation processes can be spatially and temporally modified by the local SP excitation. In the present experiment, both excitation and probing have been performed at the same site of a particle, and thus the observed spatiotemporal behavior reflects the dynamics that occur near the excitation volume. As an extension of the present method, we may develop an advanced experimental scheme where pumping and probing are spatially separated. If such a method is realized, then it may be possible to clarify how the excited electrons and energy are spatially dissipated in the particles and how e-e and e-ph scattering temporally and spatially evolve in the NR.

## References and Notes

- (1) Pohl, D. W.; Denk, W.; Lanz, M. *Appl. Phys. Lett.* **1984**, *44*, 651.
- (2) Betzig, E.; Trautman, J. K.; Harris, T. D.; Weiner, J. S.; Kostelak, R. L. *Science* **1991**, *251*, 1468.
- (3) Guest, J. R.; Stievater, T. H.; Chen, G.; Tabak, E. A.; Orr, B. G.; Steel, D. G.; Gammon, D.; Katzer, D. S. *Science* **2001**, *293*, 2224.
- (4) Matsuda, K.; Saiki, T.; Nomura, S.; Mihara, M.; Aoyagi, Y.; Nair, S.; Takagahara, T. *Phys. Rev. Lett.* **2003**, *91*, 177401.
- (5) Chicanne, C.; David, T.; Quidant R.; Weeber, J.-C.; Lacroute, Y.; Bourillot, E.; Dereux, A.; Colas des Francs, G.; Girard, C. *Phys. Rev. Lett.* **2002**, *88*, 097402.
- (6) Busbee, B. D.; Obare, S. O.; Murphy, C. J. *Adv. Mater.* **2003**, *15*, 414.
- (7) Nagahara, T.; Imura, K.; Okamoto, H. *Chem. Phys. Lett.* **2003**, *381*, 368.
- (8) Sönnichsen, C.; Franzl, T.; Wilk, T.; von Plessen, G.; Feldmann, J. *Phys. Rev. Lett.* **2002**, *88*, 077402.
- (9) Klar, T.; Perner, M.; Grosse, S.; von Plessen, G.; Spirkel, W.; Feldmann, J. *Phys. Rev. Lett.* **1998**, *80*, 4249.
- (10) Jin, R.; Charles Cao, Y.; Hao, E.; Métraux, G. S.; Schatz, G. C.; Markin, C. A. *Nature* **2003**, *425*, 487.
- (11) Girard, C.; Dereux, A. *Rep. Prog. Phys.* **1996**, *59*, 657.
- (12) Greffet, J.-J.; Carminati, R. *Prog. Surf. Sci.* **1997**, *56*, 133.
- (13) Economou, E. N. *Green's Function in Quantum Physics*; Springer-Verlag: Berlin, 1983.
- (14) Morse, P. M.; Feshbach, H. *Methods of Theoretical Physics*; McGraw-Hill: New York, 1953.
- (15) Yaghjian, A. D. *Proc. IEEE* **1980**, *68*, 248.
- (16) Weeber, J.-C.; Dereux, A.; Girard, C.; Krenn, J. R.; Groudonnet, J.-P. *Phys. Rev. B* **1999**, *60*, 9061.
- (17) Podolskiy, V. A.; Sarychev, A. K.; Shalaev, V. M. *Opt. Express* **2003**, *11*, 735.
- (18) Arbouet, A.; Voisin, C.; Christofilos, D.; Langot, P.; Del Fatti, N.; Vallée, F.; Lerne, J.; Celep, G.; Cottancin, E.; Gaudry, M.; Pellarin, M.; Broyer, M.; Maillard, M.; Pileni, M. P.; Treguer, M. *Phys. Rev. Lett.* **2003**, *90*, 177401.
- (19) Hu, M.; Hartland, G. V. *J. Phys. Chem. B* **2002**, *106*, 7029.
- (20) Link, S.; El-Sayed, M. A. *J. Phys. Chem. B* **1999**, *103*, 8410.
- (21) Hodak, J. H.; Henglein, A.; Hartland, G. V. *J. Phys. Chem. B* **2000**, *104*, 9954.
- (22) Link, S.; Burda, C.; Wang, Z. L.; El-Sayed, M. A. *J. Chem. Phys.* **1999**, *111*, 1255.
- (23) Link, S.; Burda, C.; Mohamed, M. B.; Nikoobakht, B.; El-Sayed, M. A. *Phys. Rev. B* **2000**, *61*, 6086.
- (24) Sun, C. K.; Valée, F.; Acioli, L. H.; Ippen, E. P.; Fujimoto, J. G. *Phys. Rev. B* **1994**, *50*, 15337.